

# SEM Measurement of Microporous Film Pore Distributions

Dave Biggs,<sup>1</sup> \* Shawn Jenkins,<sup>2</sup> and Rich Brown<sup>3</sup>

<sup>1</sup>Kimberly-Clark Corp., 2100 Winchester Road, Neenah, WI 54956

<sup>2</sup>Kimberly-Clark Corp., 1400 Holcomb Bridge Road, Roswell, GA 30076

<sup>3</sup>MVA Scientific Consultants, 3300 Breckinridge Blvd, Duluth, GA 30096

\*dbiggs@kcc.com

## Introduction

Microporous, breathable polymer films have been used in personal care products for several years. Two desirable properties of such films are the capacity of pores in the film to pass moisture and overall film strength. Maximizing both properties is difficult because more and larger pores tend to make the film less strong. Thus, an optimum pore structure is often sought for particular applications.

Microporous polyolefin films can be made by adding calcium carbonate ( $\text{CaCO}_3$ ) particles to the polymer [1]. Production processes, materials, and specific film properties have been previously described [2]. Newer microporous films in development have shown 50% greater breathability relative to standard control films [3]. However, adding more  $\text{CaCO}_3$  to facilitate micropore creation in films results in decreased film strength. The improved breathability was apparently afforded by a layering technology that allowed reduced  $\text{CaCO}_3$  concentration and increased strength at equivalent breathability.

In order to understand why the developmental film showed greater breathability, the distribution of pores within the film microstructure was measured. Microscopy and image analysis methods were developed to quantify changes in pore size and number distributions through the film thickness as the film manufacturing process was varied. In this article image analysis of micrographs from standard and developmental films was employed to describe these microstructural differences.

## Materials and Methods

Both test specimens were polyethylene (PE) films containing micropores and  $\text{CaCO}_3$  particles. The standard film was produced without layering, whereas the developmental film was produced with layers. Although various methods have been used over the years to characterize microporous films, such as gas permeation [4] or bubble pressure and fluid permeability [5], an alternative approach was sought that would allow visualization and quantitative measurements of the distribution of both pores and  $\text{CaCO}_3$  particles throughout the thickness of the films. This article describes a cross-sectioning method that allows both visualization and quantitative measurements. The challenge was to acquire cross-sectional images that were of high enough quality to allow clean detection and quantification of features.

**Film cross-sectioning and imaging.** In preparing a film for cross-sectional imaging, both cryo-fracturing/cutting via liquid nitrogen and sectioning with a stainless steel razor blade were initially explored. However, it was determined that the resulting cross-sectional faces produced by these techniques were problematic for subsequent image analysis because

they had rough surfaces. This roughness adversely affected the gray-scale contrast required for accurate thresholding of micro-structure features. In order to acquire smooth, clean cross sections that would have minimal topographic features, a broad ion beam (BIB) milling device was used that removes surface material and creates a “polished” cross-sectional face. Previous work had shown that related focused ion beam (FIB) techniques were useful for analyzing the sizes of micropores in cross-sectional layers [6]. In the present case, BIB-polished cross sections were subsequently gold sputter coated for 30 seconds. The cross sections were imaged in a JEOL 6490 LV SEM in high-vacuum mode at 10 kV with a 10 mm working distance. The smooth faces produced by BIB polishing removes most of the topographical contrast in backscattered electron (BSE) images of the specimen surface, allowing the BSE image to exhibit primarily atomic number contrast. Thus, in Figure 1 the pores are dark, the PE polymer is mid-gray, and the  $\text{CaCO}_3$  particles are white. This strong contrast is ideal for the image processing and analysis to follow.

Four cross sections, parallel to the films’ cross-machine direction (CD), were cut from random regions of the standard and developmental films. Each section was considered a single sampling point. Eight fields-of-view were acquired along each cross section at an instrument magnification of 1500 $\times$ .

**Image processing and analysis.** The BSE images were processed to eliminate undesirable background regions at the upper and lower surfaces of the cross sections. To accomplish

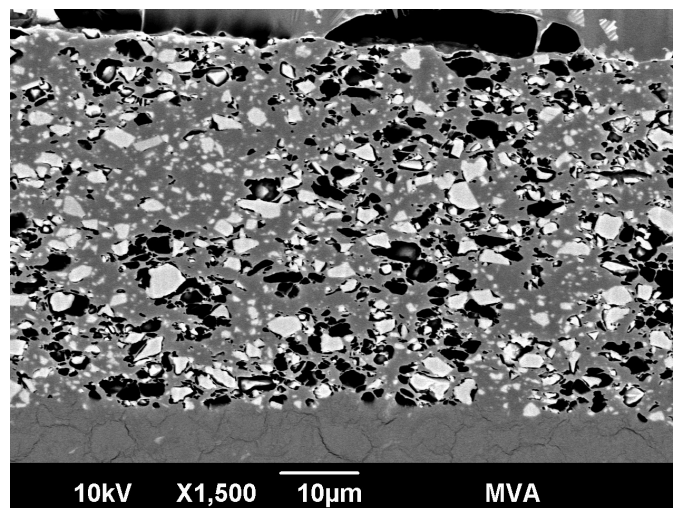


**Figure 1:** Unprocessed BSE image of the standard breathable film showing pores (dark), PE film (mid-gray), and  $\text{CaCO}_3$  particles (white). Adhesive from the copper foil tape can also be seen touching both upper and lower film surfaces (mid-gray).

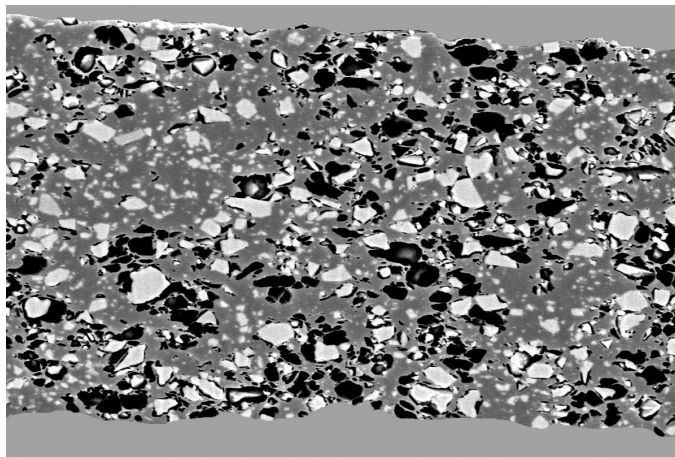


**Figure 2:** Processed BSE image of ion-milled cross section of the standard breathable film showing pores (dark), polymer film (mid-gray), and  $\text{CaCO}_3$  (white), with the images of the copper tape digitally removed. Horizontal field width =  $86\ \mu\text{m}$ .

this, ImageJ [7] was used to adjust the background regions to a common grayscale value that would not interfere with thresholding of the pores or  $\text{CaCO}_3$  particles within the cross section. Figure 2 shows a processed version of the BSE image in Figure 1.

The processed BSE images were analyzed using a Leica Microsystems image analysis software platform [8]. Three different algorithms were developed for acquiring data from the images: (1) The first algorithm was used to measure internal pore characteristics of the films, such as percent pore area and pore size, throughout the entire cross section. (2) The second algorithm measured internal pore parameters (for example, area and pore length) of films at various depths via a marching bar “slicer.” (3) The final algorithm measured the spatial distribution of the pores across film thicknesses.

Eight images were analyzed per cross-sectional cut, and the data were accumulated in Microsoft EXCEL spreadsheets. Four cross sections were analyzed for both the standard and developmental films. These data were then processed and analyzed with Student’s *t*-test comparisons because sample sizes in each data group were equivalent and a normal distribution of the data was assumed.

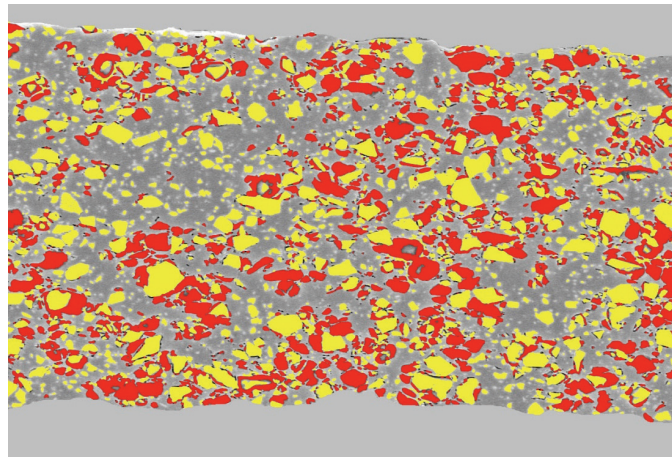
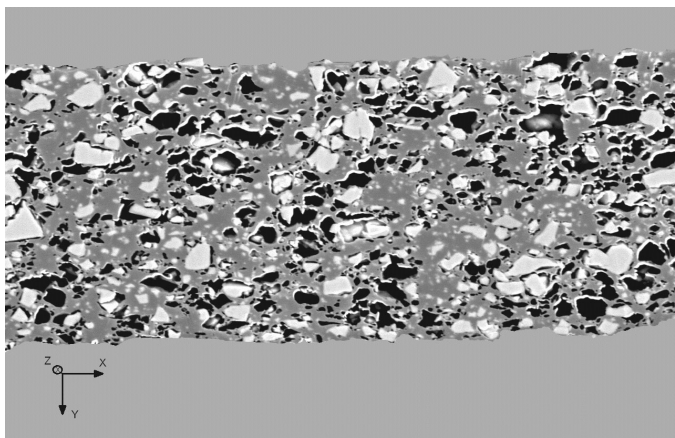


**Figure 3:** Gray-scale thresholding of pores (red) and particles (yellow) of the image in Figure 2. Horizontal field width =  $86\ \mu\text{m}$ .

## Results

Image analysis techniques for grayscale thresholding could now be applied for detecting and measuring specific features in the BSE image by harnessing the atomic number contrast [9]. Figure 3 shows the result of performing thresholding on pores and  $\text{CaCO}_3$  particles in the image of Figure 2.

**Microstructural comparisons.** Differences between the microstructures of the standard and developmental films were measured with image-analysis software. Figure 4 shows ion-milled, threshold-processed BSE images from the standard and developmental film samples. These images seem to suggest that the standard film was slightly thicker than the developmental film and that it also appeared to have lower pore density and a less regular distribution of pores in the cross-sectional thickness plane. The difference in thickness may have been related to where the sampling was performed; stretched films tend to have a thickness profile with the middle region being slightly thinner relative to the outer regions across the width of a film. That being said, the total film area measured and the number of replicates taken were large enough that it is unlikely the thickness profile affected breathability results. Also, particles and pores tend to have

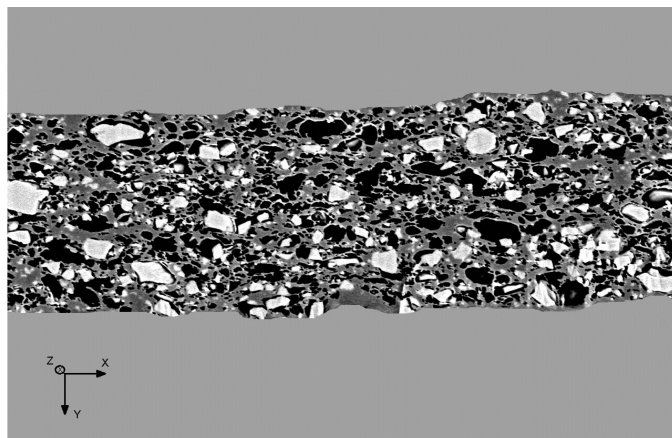


**Figure 4:** Cross sections of ion-milled unlayered standard film (left) and layered developmental film (right) at  $1,500\times$  SEM magnification. Horizontal field width =  $86\ \mu\text{m}$ .



similar distributions across the width of the film and are thus not affected by any thickness profile that may be present.

**Total internal pore volume and pore sizes.** Total pore volume (that is, pore area in the image) and individual pore sizes were measured from cross-sectional images for both films. These results are summarized in Table 1. A histogram illustration comparing the total percentage of pore volume data between the films is shown in Figure 5. These data suggested that the developmental film possessed a higher percentage of pore volume (that is, % pore area); whereas, the average pore size was not statistically different.

However, differences between the % pore area mean values were not found to be significantly different, as shown by the Student's *t*-test analysis of the data in Table 1. The overlap between the ranges indicated that the respective mean values were not significantly different from each other, although the developmental film obviously trended somewhat higher in pore volume than the standard film. Data were compared at the 90% confidence level.

**X-Y-plane cross-sectional thickness pore distributions.** Because the initial observations of film cross sections suggested that the developmental film possessed a more uniform distribution of its pores throughout the cross-sectional thickness, image analysis algorithms were developed and applied to the cross-sectional images.

For both thickness and pore count per mm of thickness parameters, eight individual measurements were performed on each of the cross sections to arrive at a mean value per section. The four cross-sectional mean values were then compared in the Student's *t*-test analyses. The measurements of film thickness and the number of pores in the cross-sectional plane are summarized in Table 2.

These data showed that differences existed between the films for the pore count per thickness data. The gap between Student's *t*-test confidence limit ranges for pore count confirmed that the developmental film had a higher pore density than the standard film. Although the standard film's thickness trended higher than that of the developmental, this may have been at

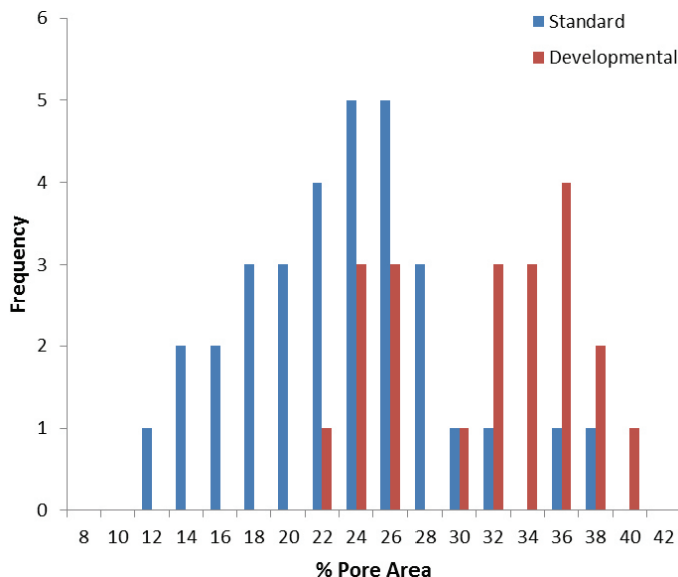


Figure 5: Histogram of % pore area data showing that the developmental film has a greater pore area (pore volume).

least partially influenced by where the film was cross-sectioned during sample preparation.

In order to measure the variation of pore parameters in the films' cross-sectional thickness planes, a pseudo depth "slicer" of 1 μm thickness was used to progress through the sections from the film's upper surface through to the lower surface. An illustration of how this worked is shown in Figure 6. In this image, the X horizontal direction represents the cross-machine direction of the film, whereas Z, which is into the image plane, represents the film's machine directionality. The Y vertical direction represents the film thickness. Both pore area and diameter were measured at each slice location down through the thickness (Y) of the film. The data were then analyzed for pore area and pore size variation by calculating the % coefficient-of-variation (%COV) for each parameter at each of the selected thickness depth locations. Note that data from the initial slices at surface interfaces of both films were not included in the calculations. The thickness-pore variation data are summarized in Table 3. These data showed that the standard film possessed higher variation (that is, %COV) in pore volume, through the film thickness, and a higher variation in pore size than that of the developmental film.

### Discussion

The fact that the pore count per thickness density (Table 2) was found to be higher for the developmental film corroborates with the observation that this film also had 50% greater breathability

Table 1: Internal pore volume and size data for breathable polymer films.

Sample ID	Total Pores			Individual Pore Size	
	% Pore area*	S. Dev.	Student's <i>t</i> -test Ranges	Diameter (μm)	S. Dev.
Standard	22.2	6.2	15.0–29.5	1.53	0.16
Developmental	29.8	6.5	18.8–40.8	1.42	0.06

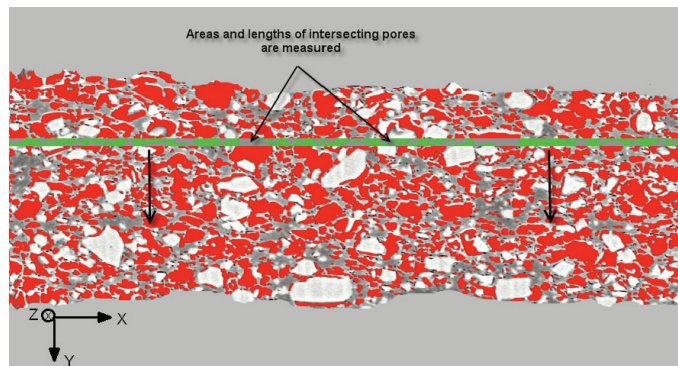
\*For any given specimen thickness, pore area is indicative of pore volume.

Table 2: Film thickness and pore count for breathable polymer films.

Sample ID	Thickness & # Pores/Thickness Depth					
	Thickness (μm)	S. Dev.	Student's <i>t</i> -test Ranges	Pore number per μm of thickness	S. Dev.	Student's <i>t</i> -test Ranges
Standard	40.8	4.8	35.2–46.5	128	6.6	120–136
Developmental	26.4	5.6	17.0–35.9	195	25.2	153–238

**Table 3:** Through-thickness pore variation data for breathable polymer films.

Sample ID	Through-Thickness Pore Variation					
	Pore area %COV	S. Dev.	Student's t-test Ranges	Diameter %COV	S. Dev.	Student's t-test Ranges
Standard	24.0	4.1	19.2–28.7	14.0	0.4	13.6–14.5
Developmental	15.6	2.9	10.7–20.4	10.8	0.4	10.1–11.5



**Figure 6:** Thickness depth slicer intersecting detected pores for measurements. Horizontal field width = 86  $\mu$ m.

than the standard. This is also in line with the trend showing that the developmental film had more overall cross-sectional % pore area (Table 1) than the standard, even though the sizes of individual pores were found to be comparable. It is possible that there is greater connectivity between pores in the layered film because of the higher density value.

Because the variation (%COV) in both pore diameter and volume through the film thickness were found to be higher for the standard film, this suggested that the developmental film's production layering process may have contributed to better mixing of the CaCO<sub>3</sub> particles. Thus, pores were more evenly distributed throughout the thickness of the developmental film. This finding confirmed our initial visual observations that the layered developmental film appeared to have a more uniform distribution of pores throughout its thickness relative to the unlayered, standard film.

**Conclusions**

A combination of ion milling cross-sectional polishing and backscattered electron (BSE) imaging techniques provided a means of generating high-contrast images, which were useful for quantitative image analysis. Using these techniques on breathable microporous films, a layered developmental film was found to possess a higher pore count per thickness and a more uniform distribution of pores throughout its thickness depth than an unlayered standard film. These findings suggested that the developmental film manufacturing process resulted in more uniform mixing of the CaCO<sub>3</sub> particles, resulting in pores that were more closely and evenly spaced.

**References**


[1] A McCormack, R Palmer, and C Shea, US Patent US7932196 B2, *Microporous stretch thinned film/nonwoven laminates and limited use or disposable product applications*, April 26, 2011.

[2] C Mueller et al., *J Appl Polym Sci* 78(4) (2000) 816–28.  
 [3] SE Jenkins, US Patent Application 2012/0288695 A1, *Multilayer Breathable Films*, November 15, 2012.  
 [4] S Nagō et al., *J Appl Polym Sci* 45(9) (1992) 1527–35.

[5] S Ran, W Zhu, and M Xu, "Determination of Average Pore Size and Size Distribution of a Polypropylene Microporous Film by the Combination Method of Bubble Pressure and Fluid Permeability," *Acta Polym Sin* 1999–2001, [http://en.cnki.com.cn/Article\\_en/CJFDTOTAL-GFXB901.019.htm](http://en.cnki.com.cn/Article_en/CJFDTOTAL-GFXB901.019.htm).  
 [6] T Okayasu, S Kusama, E Tozaki, and T Miyagawa, "Analysis of the Real Microstructure of the Cross Section of a Coated Layer Prepared by FIB - Novel Method for Micropore Size Distribution Measurement," *Proceedings of the 2001 TAPPI Coating and Graphic Arts Conference and Trade Fair*, San Diego, CA, May 2003, 183–92.  
 [7] The ImageJ website is <http://rsbweb.nih.gov/ij>.  
 [8] QWIN Pro Version 3.5.1, April 2008, Leica Microsystems Ltd., Heerbrugg, Switzerland.  
 [9] JI Goldstein et al., *Scanning Electron Microscopy and X-ray Microanalysis*, Springer, New York, 2003.

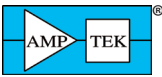
MT

## Amptek FAST SDD™ for SEM-EDS Applications



Amptek's new line of SDD detectors for EDS use with SEMs utilizes new technology "C Series" X-ray windows (Si<sub>3</sub>N<sub>4</sub>) and has a low energy response down to Carbon. With its high intrinsic efficiency the SDD is ideal for EDS XRF. See why Amptek detectors are the #1 choice of OEMs worldwide.

Transmission for Low Z Elements	
B	19.7%
C	43.9%
N	59.2%
O	62%
F	69%
Ne	72.9%
Na	75.1%
Mg	77.3%
Al	80.3%
Si	81.8%



**OEM's #1 Choice**

[www.amptek.com](http://www.amptek.com)

